Progress in Additive Manufacturing
https://doi.org/10.1007/s40964-024-00617-w

FULL RESEARCH ARTICLE

Factors affecting interface bonding in multi-material additive manufacturing

Sarah Delia[1] · Arif Rochman[1] · Albert Curmi[1]

Received: 30 October 2023 / Accepted: 23 March 2024

Abstract
Additive manufacturing or 3D printing is the process of depositing material layer-by-layer to create 3-dimensional products. When creating 3D-printed products from two or more materials, multi-material additive manufacturing processes are used which eliminate the need for assembly operations. Fused filament fabrication multi-material additive manufacturing permits the production of a single printed item employing multiple materials in fused filament fabrication. This work studied the factors affecting fused filament fabrication multi-material additive manufacturing, by reviewing existing works, designing part(s), conducting design of experiments, and carrying out parts' performance test. An E3D multi-material filament 3D printer was utilised throughout this study. The chosen polymer combination was polycarbonate (PC) and poly(methyl methacrylate) (PMMA), whilst the design and testing of the multi-material parts was limited to lap-shear testing. Results showed that the interface bonding of the PMMA/PC (PMMA printed first and followed by PC) specimens was stronger than the one of the PC/PMMA specimens. Furthermore, to investigate the effect of the contact or overlapping area on the interface bonding strength, PMMA/PC specimens with varying dimensions were designed, printed, and tested. When the contact area was reduced, a strong interface bonding between the PMMA and PC layers was still maintained.

Keywords Additive manufacturing · Fused filament fabrication · Multi-material additive manufacturing · Interface bonding · Lap-shear testing · Shear strength

1 Introduction

The ISO/ASTM 52900 standard [1] defines additive manufacturing (AM) as the fabrication of products through the addition of materials layer by layer from solid computer-aided design (CAD) models. AM is used for rapid prototyping and the production of final products due to its high efficiency [2]. The seven AM technology categories include binder jetting, directed energy deposition, material extrusion, material jetting, powder bed fusion, sheet lamination, and vat photopolymerisation. In this work, fused filament fabrication (FFF) was investigated which is an extrusion-based AM process [1]. Multi-material additive manufacturing (MMAM) techniques produce parts made up of two or more materials, which avoids assembly work of separately manufactured components [3]. MMAM products find their applications in the biomedical, robotics, and electronic fields [4].

The literature reviewed relating to FFF and FFF MMAM showed that only a few MMAM studies have been conducted, especially in the selection of materials to combine. The research carried out by Li et al. [5] and Rajpurohit and Dave [6], used single material FFF, where both concluded that lower layer thickness values resulted in greater tensile strength and bonding strength since less heat was required for adjacent strands to bond. Previous works have identified that several processing parameters have an influence on the quality and strength of multi-material specimens. However, they were limited to mainly raster angle, printing speed, nozzle diameter, printing order, infill pattern, infill density, and machine calibration [2, 7–9]. Other research studies such as the work by Freund et al. [10] determined the influencing factors on MMAM using different material

✉ Arif Rochman
arif.rochman@um.edu.mt

Sarah Delia
sarah.delia.19@um.edu.mt

Albert Curmi
albert.curmi.16@um.edu.mt

[1] Department of Industrial and Manufacturing Engineering, University of Malta, Msida 2080, MSD, Malta

Published online: 19 April 2024

combinations; however, it only analysed the factors which are written in bold as shown in Fig. 1 and reasons for those selections were not given. Yap et al. [9] fabricated tensile and flexural specimens using acrylonitrile butadiene styrene (ABS) and PC, and examined the printing speed, infill density and nozzle diameter printing parameters, to understand PC's effect on the mechanical properties of MMAM parts. It was concluded that an increase in printing speed reduced the mechanical properties, whilst larger nozzle diameter improved them. In addition, greater infill density values enhanced the flexural strength and flexural modulus, however, reduced in elongation.

In some works, parameters such as layer thickness and number of perimeter shells were taken as constant values [4]. In this work, all factors were first still taken into consideration since their effects could differ from one to another application. Specimens of various designs were developed to perform various mechanical tests, such as tensile, lap-shear, and compression testing. The process parameters and quality of specimens influences the type of adhesion mechanism.

This study delves into the underlying mechanisms and factors that influence the interlayer bonding strength and quality of the bonds between the different materials in a multi-material 3D-printed product. Following a research methodology adopted from Duffy and O'Donnell [11], a comprehensive approach is employed, encompassing a literature review, selection analysis, experiments, and conclusions. Since there are similarities between welding and MMAM, several polymer material combinations which consist of compatible polymers, including polymers blending miscibility, were identified. However, for this study, there were research boundaries such as the MMAM limited to polymer-based FFF using the available filaments on the market, only one material combination used, the E3D printer utilised without a heating chamber, and mechanical testing limited to lap-shear testing to determine the interface bonding strength. For originality and advancement of research in the FFF MMAM, it was ensured that the material combination selected had not been previously explored and a new specimen design was created to understand the influence of the selected printing parameters. Finally, suggestions were proposed for future work to expand knowledge on FFF MMAM technologies.

2 Materials and methods

2.1 Materials

Possible material combination pairs were evaluated based on the material compatibility and blending miscibility. Screening of the material combinations was then carried out using the following criteria: the pair not yet studied, material availability in filament form, the materials not from similar monomers, their processing temperature below the maximum temperature of the printer's nozzles, and both materials possessing different material properties in terms of toughness and brittleness, as shown in Table 1. Material pairs that include polymers as a polymer group such as thermoplastic elastomers (TPE*) were eliminated since TPE includes different thermoplastic elastomers such as thermoplastic polyurethane and thermoplastic polyolefins, and hence, the type of TPE could not be determined. Since the material combination polycarbonate (PC) and poly (methyl methacrylate)

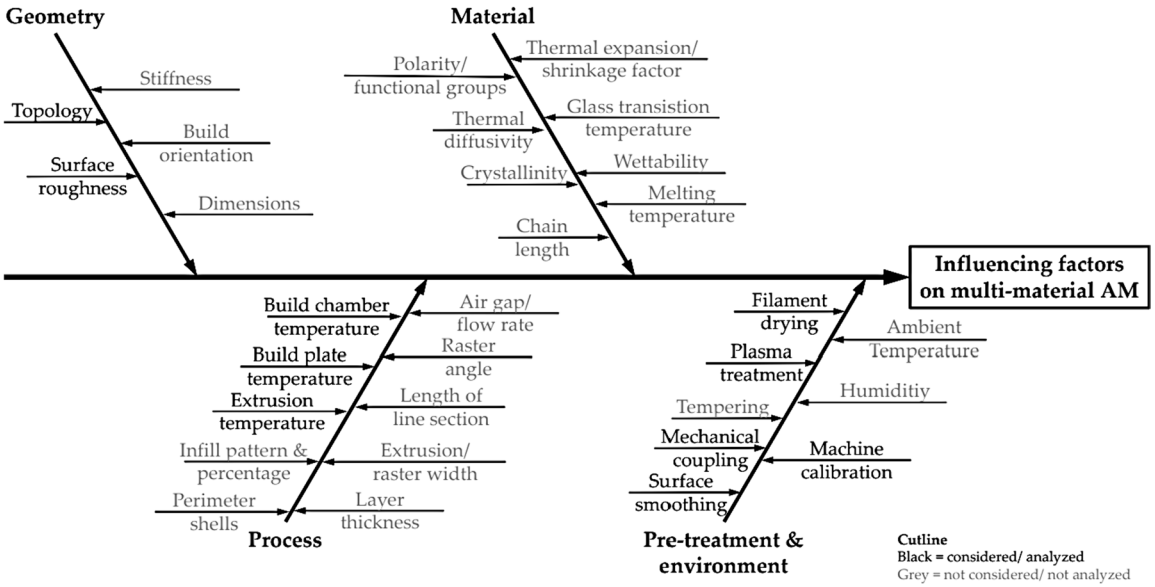

Fig. 1 Ishikawa diagram showing the influencing factors on multi-material AM [10]

Table 1 Material combination selection

Material combination	Not yet studied	Available in filament	Not from similar monomers	Within E3D processing temperature	Different material properties (brittle and tough)
ABS/ASA	✓	✓	×	✓	×
ABS/MABS	✓	✓	×	✓	×
ABS/PBT	✓	×	✓	✓	✓
ABS/PC	×	✓	✓	✓	×
ABS/PMMA	✓	✓	×	✓	✓
ABS/SAN	✓	×	×	✓	✓
ABS/TPE*	✓	✓	✓	✓	✓
ABS/PA	✓	✓	✓	✓	×
ASA/PBT	✓	×	✓	✓	✓
ASA/SAN	✓	×	×	✓	✓
PBT/PC	✓	×	✓	✓	✓
PBT/SAN	✓	×	✓	✓	×
PC/PMMA	✓	✓	✓	✓	✓
PC/SAN	✓	×	✓	✓	✓
LDPE/PP	✓	✓	✓	×	×
PES/PSU	✓	✓	×	×	×
PMMA/SAN	✓	×	✓	✓	×
PP/TPE*	✓	✓	✓	✓	✓
PPS/PC	✓	✓	✓	×	✓
PS/PPO	✓	×	✓	✓	×

✓ *material pair meets criteria*
× *material pair does not meet criteria*

(PMMA) fulfilled the above criteria, they were then chosen as the material pair for this study. The filaments chosen were a black ePC by eSUN (Shenzhen, China) and a red transparent PMMA by Devil Design (Mikołów, Poland).

2.2 Methods

2.2.1 3D-printing setup

A 3D-printing system by E3D (London, United Kingdom) was used for this study which is equipped with four different tools/printing heads and a tool changer, which allows the tool changeover to produce multi-material parts in one printing cycle. Figure 2 shows the assembled E3D printer. The PrusaSlicer software was the slicer software utilised throughout this study. Machine calibration was carried out to enable the fabrication of prints with the desired dimensional accuracy and specifications. Calibrating the E3D printer consisted of homing and tool change configurations, PID tuning of the heaters, bed levelling and automatic bed mesh levelling, and adjusting the Z-, X- and Y-offsets. In addition, custom G-codes were incorporated into the setting of the printer to carry out prime lines and purging after the completion of a tool change. E-step calibration followed

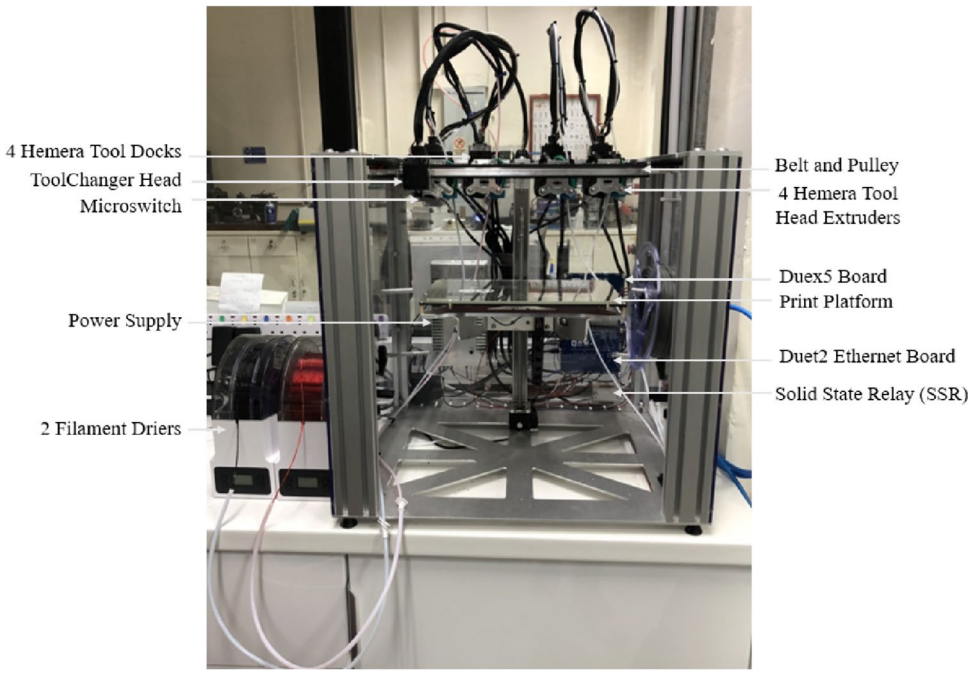

Fig. 2 Assembled tool changer and motion system including a tool changer and four Hemera filament extruders

by extrusion multiplier calibration was also completed to modify the actual amount being extruded out of the nozzle of the printing heads.

PC and PMMA are both hygroscopic polymeric materials and hence it was ensured that filament drying was completed before initiating the prints [12, 13]. Two eBOX Lite filament dryers by eSUN (Shenzhen, China) were used to pre-heat and dry both filaments before and during 3D printing with the following parameters: 6 h at 80 °C for PC and 6 h at 75 °C for PMMA filament. Issues regarding adhesion of the polymer layers to the printing bed were present; therefore, after cleaning the printer bed with isopropyl alcohol, a thin layer of an adhesive polyvinyl acetate glue was added to the bed before each print.

2.2.2 Design of testing specimen

Since the interface bonding strength of the chosen PC and PMMA material combination for FFF MMAM was unknown, two specimen designs were created and named as Design A and Design B. Design A was mainly to investigate the influence of the printing approach in terms of the movement of the nozzle and was created based on the dimensions of the ASTM D3163 standard, as shown in Fig. 3. This is a standard test method for determining strength of adhesively bonded rigid plastic lap-shear joints in shear by tension loading [14]. Whilst the overlap length was increased for a higher contact/overlapping area of the inter layers, the overall length of the specimen was reduced to decrease the printing time. The dimensions of Design A are shown in Fig. 4.

Design B was created also based on the ASTM D3163 standard, as shown in Fig. 5, with such modifications that the second material will be printed directly on the overlapping area where shear would be tested. The design also resulted in the second material having a lower volume to be printed due to the removal of the tab from the original standard lap-shear sample and does not consist of overhung material. Design B was used to conduct the design of experiments and

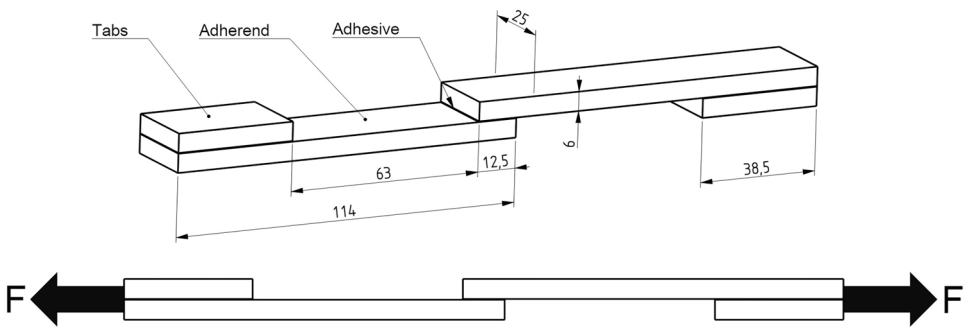

Fig. 3 Standard test dimensions following the ASTM D3163 standard [14]

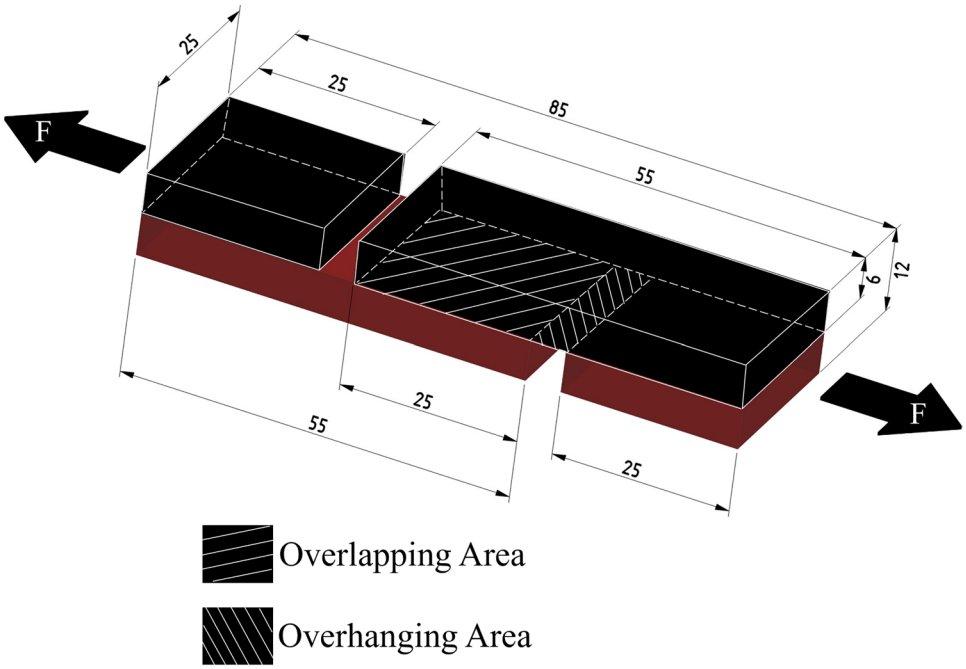

Fig. 4 Dimensions of Design A with an increased overlapping area to 25 × 25 mm^2 and a decreased overall length to 85 mm resulting in a small overhanging gap of 5 mm

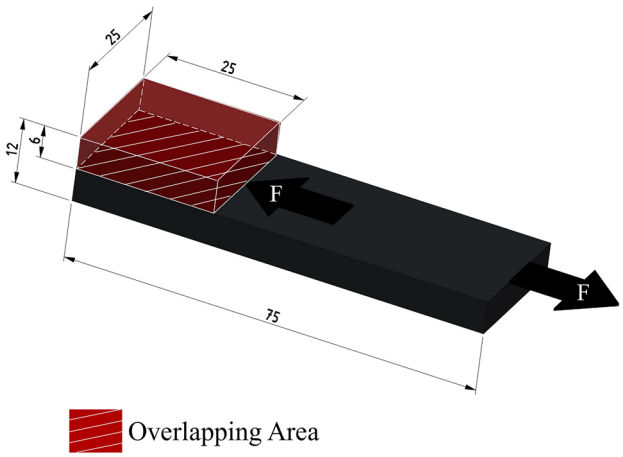

Fig. 5 Dimensions of Design B with an overlapping area of 25 × 25 mm^2

to investigate the effect of overlapping/contact area for the processing parameters and printing order which resulted in the highest bonding strength. For the latter test, the overlapping area of Design B was gradually decreased.

2.2.3 Printing experiment

Eight factors were analysed to determine which parameters are to be utilised in the design of experiments (DOE). Layer thickness and raster width were selected whilst the other parameters were given constant values throughout all the prints as shown in Table 2. The levels for each factor were then determined.

Table 2 Constant printing parameters

Printing parameters	
Raster angle/infill line direction (°)	0
Infill density (%)	100
Infill pattern	Aligned rectilinear
Extrusion/processing temperature (°C)	
PC	250
PMMA	235
Extrusion multiplier	1
Build plate temperature (°C)	90
Printing speed (mm/s)	60

Layer thickness Layer thickness, also referred to as layer height, describes the thickness or height of each deposited layer along the *z*-axis of the printed item. The layer thicknesses were selected to be less than the nozzle diameter, ranging from 25 to 80% of the nozzle diameter or half the nozzle diameter [15]. The E3D printer's nozzle used was 0.4 mm in diameter [16]. As a result, the chosen layer thicknesses were 0.1 mm (25% of the nozzle diameter) as the minimum level value, and 0.2 mm (50% of the nozzle diameter), as the maximum level value of this factor.

Raster width and raster angle The raster width, also known as the infill line width, is typically set at the nozzle diameter; however, in this case, greater interface bonding required taking 120% of the nozzle diameter, resulting in a width of 0.48 mm ≃ 0.5 mm [17]. Therefore, 0.5 mm and 0.4 mm were chosen as the maximum and minimum

levels of this factor. The raster angle of 0° was taken at a constant value to be able to test the highest expected strength during the lap-shear testing. With a raster angle of 0°, the extruded strands would be aligned parallel to the direction of loading during lap-shear testing, and hence would maximise their ability to resist the applied force.

The printing order in multi-material specimens was also an important factor and was taken into consideration by the generation of two DOEs for the two printing orders: PC followed by PMMA (order designation PC/PMMA) and PMMA followed by PC (order designation PMMA/PC). A 1/2 2-level fractional factorial resolution IV design was used for each printing order, resulting in 8 runs. The factors and their respective levels and the DOEs for each run of both printing orders are listed in Tables 3 and 4, respectively. Each run was repeated three times to obtain accurate results and reduce overall experimental errors.

A Python file was developed to enable the printing of multiple specimens with the same factors and levels using a single G-code. With this file, each lap-shear specimen may be completed utilising both materials before proceeding on to the next specimen.

2.2.4 Lap-shear testing

Mechanical testing was conducted using the Testometric M350-20CT (TestometricTM, Lancashire, England) tensile testing machine with a 20 kN load cell and steady rate of tensile force was applied. The EN ISO 527-1:2012 [18] for determination of tensile polymer properties was followed where a test speed of 2 mm/min was selected, which was the same speed utilised in another study [7].

A customised tensile puller was created to carry out the lap-shear tests of the new specimen. The puller was designed in such a way so as to allow symmetrical pulling of the specimen from the centre of the part, i.e. the interface between the first and second material. The puller was made to accommodate the machine and replace the standard tensile grippers. Clearances and semi-circular holes were incorporated into the design to account for any warpage as well as to address any potential dimensional errors that could occur whilst printing the specimens. To ensure symmetrical testing, an additional aluminium block was machined and attached to the other side of the specimens during testing to compensate for the thickness of the specimen. Figure 6 depicts the design and assembly of the puller, the block, and the testing specimen during the lap-shear testing.

3 Results and discussion

3.1 Failure modes

No standards or terminology on the failure modes of lap-shear specimens are currently available for additively manufactured polymer parts. The likely failure modes of

Table 3 Factors and their respective levels for PC/PMMA and PMMA/PC

Factors	PC/PMMA				PMMA/PC			
	PC		PMMA		PMMA		PC	
	Max	Min	Max	Min	Max	Min	Max	Min
Layer thickness (mm)	0.2	0.1	0.2	0.1	0.2	0.1	0.2	0.1
Raster width (mm)	0.5	0.4	0.5	0.4	0.5	0.4	0.5	0.4

Table 4 PC/PMMA and PMMA/PC DOE

Run no.	PC/PMMA				PMMA/PC			
	PC layer thickness (mm)	PC raster width (mm)	PMMA layer thickness (mm)	PMMA raster width (mm)	PMMA layer thickness (mm)	PMMA raster width (mm)	PC layer thickness (mm)	PC raster width (mm)
1	0.2	0.4	0.1	0.5	0.2	0.4	0.1	0.5
2	0.1	0.4	0.2	0.5	0.1	0.4	0.2	0.5
3	0.2	0.5	0.2	0.5	0.2	0.5	0.2	0.5
4	0.2	0.4	0.2	0.4	0.2	0.4	0.2	0.4
5	0.1	0.4	0.1	0.4	0.1	0.4	0.1	0.4
6	0.2	0.5	0.1	0.4	0.2	0.5	0.1	0.4
7	0.1	0.5	0.1	0.5	0.1	0.5	0.1	0.5
8	0.1	0.5	0.2	0.4	0.1	0.5	0.2	0.4

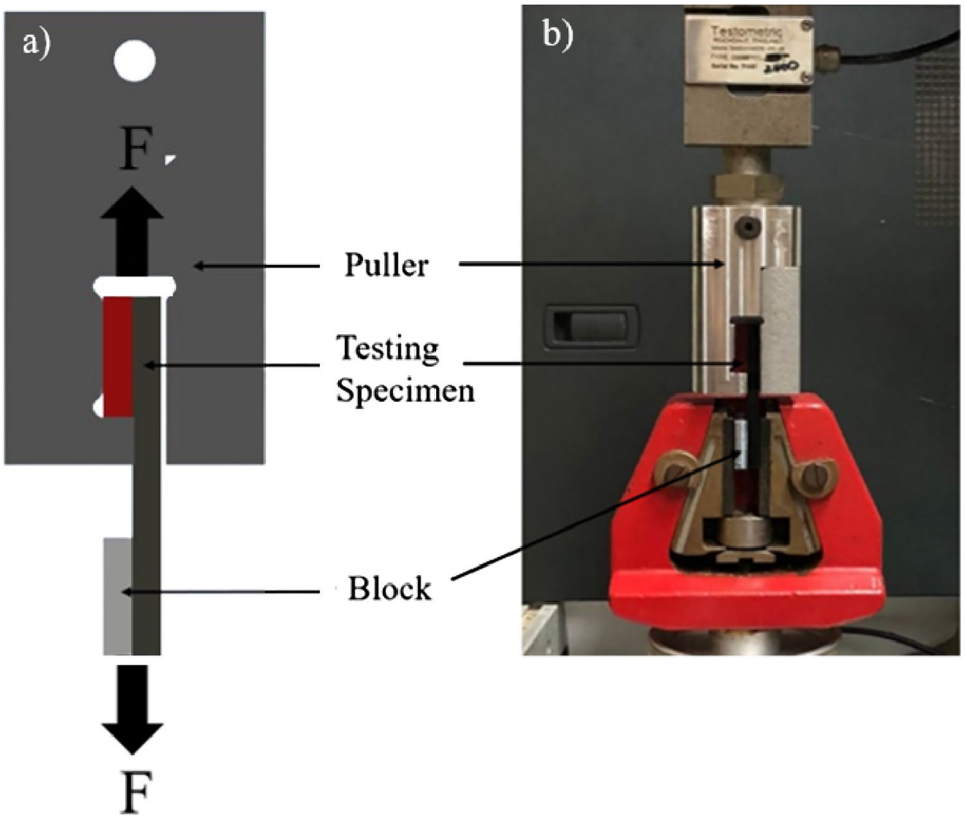

Fig. 6 **a** CAD model of puller, block, and testing specimen and **b** assembly of puller, block, and testing specimen in the Testometric M350-20CT tensile testing machine

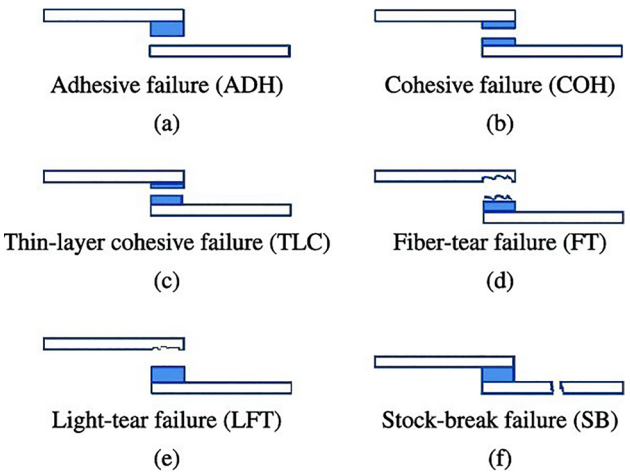

Fig. 7 Typical failure modes of lap-shear specimens [19]

adhesive lap-shear specimens are shown in Fig. 7. However, the terminology could be utilised and altered such that adhesive failure was referred to as interface failure, light-fibre-tear failure as layer-tear failure and stock-break failure kept the same terminology [19].

3.2 Visual analysis

The DOE specimens were visually inspected to identify the optimal printing parameters and determine whether the prints were repeatable. It is important to note that the first two specimens (A and B) were printed consecutively in the same printing cycle, whilst the third specimen (C) was printed separately. The results of each run for both the printing orders, PC/PMMA and PMMMA/PC are shown in Tables 5 and 6 respectively.

Specimen C from run 4 of the PC/PMMA printing order and specimen C from run 3 of the PMMA/PC order had good surface quality. In contrast, other specimens showed mixed surface quality, with some having one material with a high surface finish and the other with a poor surface finish. Some specimens had rough surface finishes for both materials.

The use of a 0.1 mm layer thickness in the PMMA/PC printing order resulted in lower surface quality for both materials. Bulges or bumps were observed in the middle of the second material in some prints, caused by the PMMA material at a 0.1 mm layer thickness. Warping at the corners occurred due to material shrinkage during printing, even though a brim was incorporated into the design of each specimen.

Table 5 Top and side views of PC/PMMA specimens

	Specimen A	Specimen B	Specimen C
Run 1			
Run 2			
Run 3			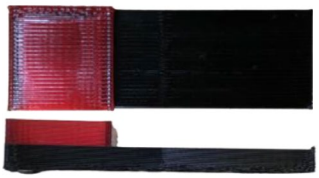
Run 4			
Run 5			
Run 6			
Run 7			
Run 8	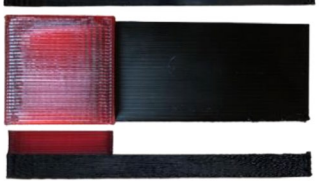		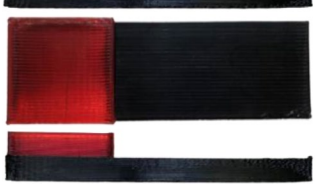

3.3 Dimensional analysis

A Mitutoyo Digimatic Indicator 543-515-1 IDF-150 (Japan) with a resolution of 0.001 mm was used to measure the thicknesses of the printed specimens, due to its influence on the bonding strength. These measurements revealed whether the print had decreased or increased in size. The first material may have shrunk or increased in size during the tool change or printing, influencing the position of the second material's first layer. The second material's position could affect the interface bonding between the two materials. Figure 8 shows the location and order of the readings taken.

Table 6 Top and side views of PMMA/PC specimens

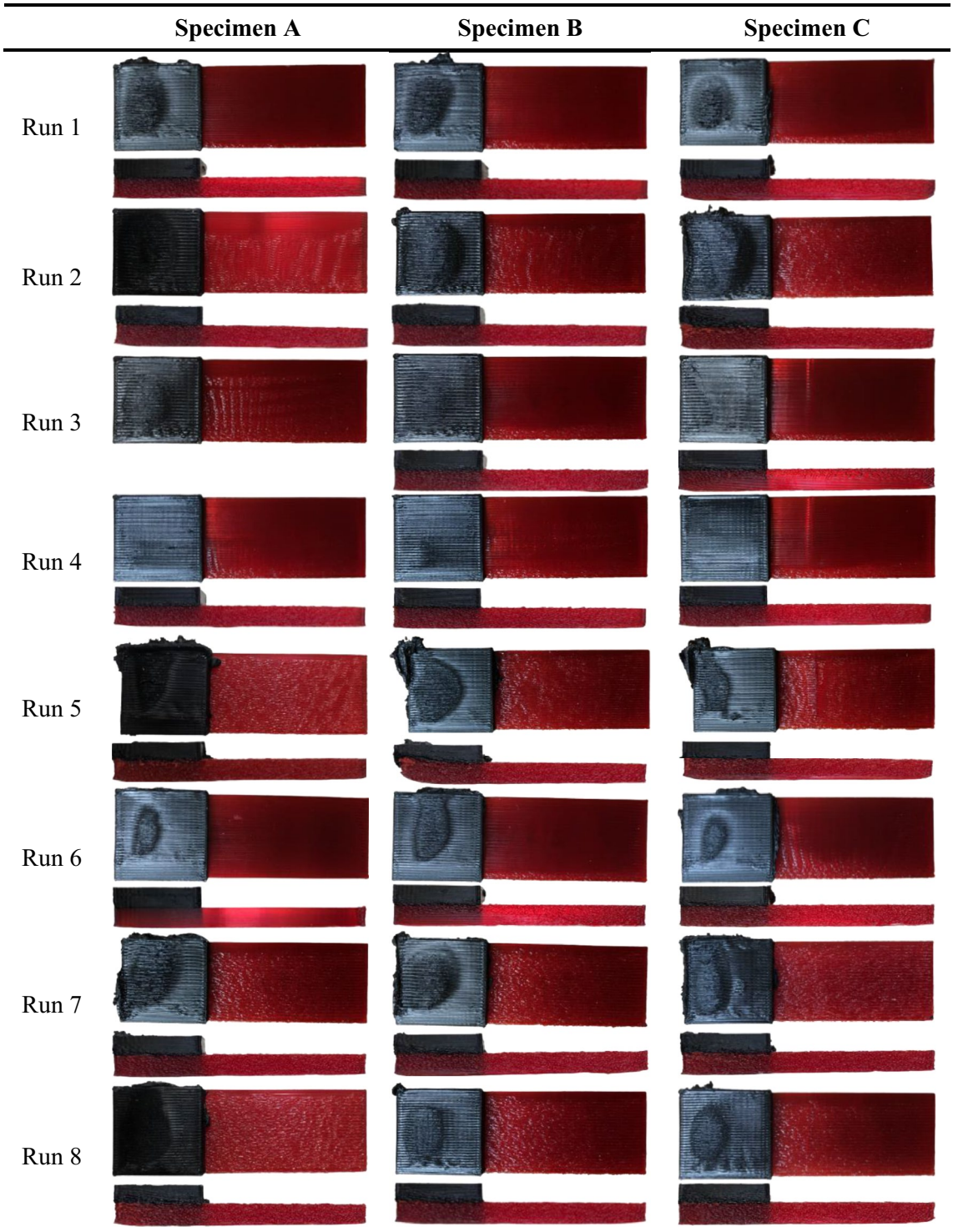

Figures 9 and 10 show bar charts of the average thicknesses and standard deviations for both printing orders of the material combination. It was observed that in the PC/PMMA printing sequence, the thickness of the first material printed (PC), was consistent throughout and that none of the average values were less than 6 mm, independent of the process parameters of each run. In the PMMA/PC printing order, the thickness of the first material (PMMA) varied, with most specimens having average thicknesses larger than 6 mm, although runs 1 and 4 had average thickness values less than 6 mm.

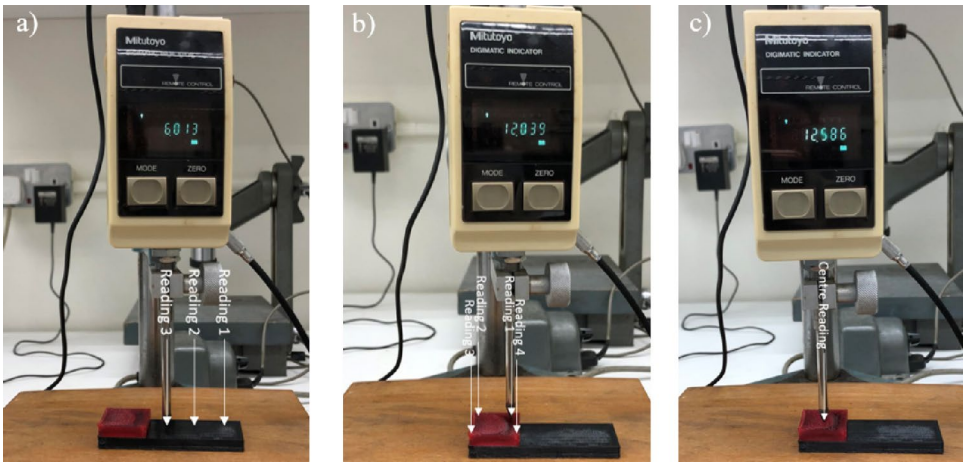

Fig. 8 Measurement positions of **a** first material thicknesses, **b** and **c** total specimen thickness

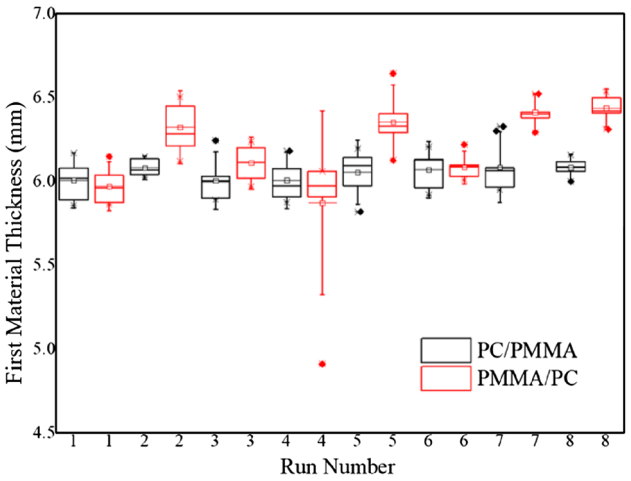

Fig. 9 Box plot of first material thickness against run number

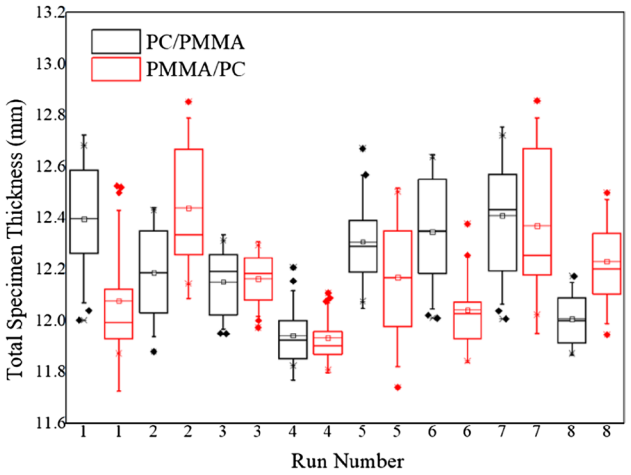

Fig. 10 Box plot of total specimen thickness against run number

When comparing the two printing orders, more accurate thicknesses of the first material were obtained when printing PC first than when printing PMMA first. The optimal run for both printing orders was run 6 as it generated the first material of the specimen as required, i.e. a thickness of roughly 6 mm. Similarly, due to the addition of thicker PMMA material, most of the runs of the PC/PMMA printing order resulted in an overall thickness larger than 12 mm. In terms of overall thickness, run 4 for both printing orders resulted in values less than 12 mm. Overall, the optimal specimens had a total thickness of 12.007 mm and were printed in run 8 of the PC/PMMA printing order.

3.4 LAP-shear analysis

3.4.1 Lap-shear tests of PC/PMMA

The different runs produced different values of force, elongation, and strength, depending on the process parameters used and dimensional accuracies achieved. Interface failure and layer-tear failure modes were experienced throughout all the specimens of the printing order PC/PMMA. It was concluded that the shear strength of this printing order was lower than the tensile strength of PC, which according to its material datasheet is 54.88 MPa, since the major failure mode was interface failure [20]. The highest shear strength was achieved by the specimens of run 7 with an average shear strength of 7.573 ± 4.957 MPa, i.e. only 13.8% of PC's tensile strength. These specimens were printed using the same printing parameters for both materials i.e. the lowest layer thickness (0.1 mm) and highest raster width (0.5 mm). This highest interface bonding resulted from the highest contact area created by the same and highest raster width and accompanied by the same and lowest layer thickness. As stated in Li et al. [5] and Rajpurohit and Dave [6], a lower

layer thickness resulted in greater bonding strength due to the high amount of heat which aided the melting and fusing of the deposited layer to the previous layer. However, the lowest shear strength was obtained using different printing parameters for each material, i.e. where PC was printed with a layer thickness of 0.2 mm and a low raster width of 0.4 mm, followed by a layer thickness of 0.1 mm and a raster width of 0.5 mm for PMMA. This difference in printing parameters resulted in less contact area at the interface due to the difference in raster widths.

A Pareto chart was plotted to determine the most influencing factors of the PC/PMMA specimens in shear strength as shown in Fig. 11. It was concluded that all the factors could be considered equally significant since none of the factors exceeded the reference line at 3.182, which is the t-quantile of the t-distribution, identified using the Minitab software.

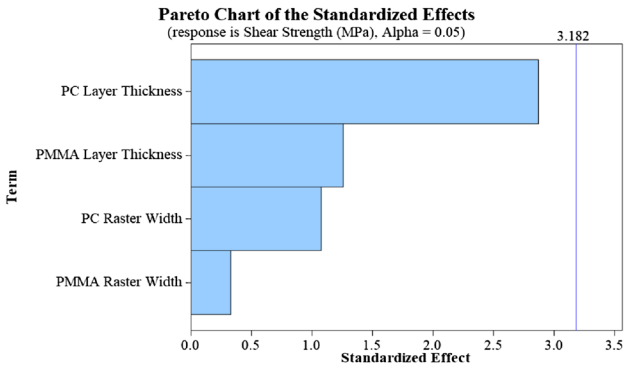

Fig. 11 Pareto chart for shear strength of the PC/PMMA specimens

The mean response value was applied to the maximum and minimum levels of each factor in the main effects plot to highlight the relationship between the factors and the shear strength. Figure 12 shows that the PC layer thickness was a significant factor for the PC/PMMA specimens. In addition, the shear strength was enhanced by lower PC layer thickness values and greater PC raster width and PMMA layer thickness values. The shear strength was barely affected by the variations in raster width of PMMA. The ideal combination of factors for this printing order would be 0.1 mm and 0.2 mm for PC and PMMA layer thickness, respectively, and 0.5 mm for both PC and PMMA raster width.

Figure 13 shows the generated interaction plot for the PC/PMMA specimens, where the influence of one factor is dependent on the level of another factor. The raster width of PC had strong interactions with both the layer thickness and raster width of PMMA. Further examination of the interaction plot between PC raster width and PMMA layer thickness indicated that shear strength was greatest when raster width was kept high and layer thickness was kept low. The interaction plot between the raster widths of PC and PMMA revealed that shear strength was greatest when both raster widths were at their maximum. There were no interactions found between the other factors.

Most of the specimens of runs 1, 2, 3, 4, 5, and 8, exhibited interface failure. This type of failure was characterised by a clean cut at the interface area. However, some of the specimens had the materials remaining in contact at the corners. The occurrence of this failure mode could be attributed to the print quality or the influence of the process parameters which fabricated these runs. However, run 6 displayed diverse failure patterns. Some specimens experienced

Fig. 12 Main effects plot of the factors on shear strength of the PC/PMMA specimens

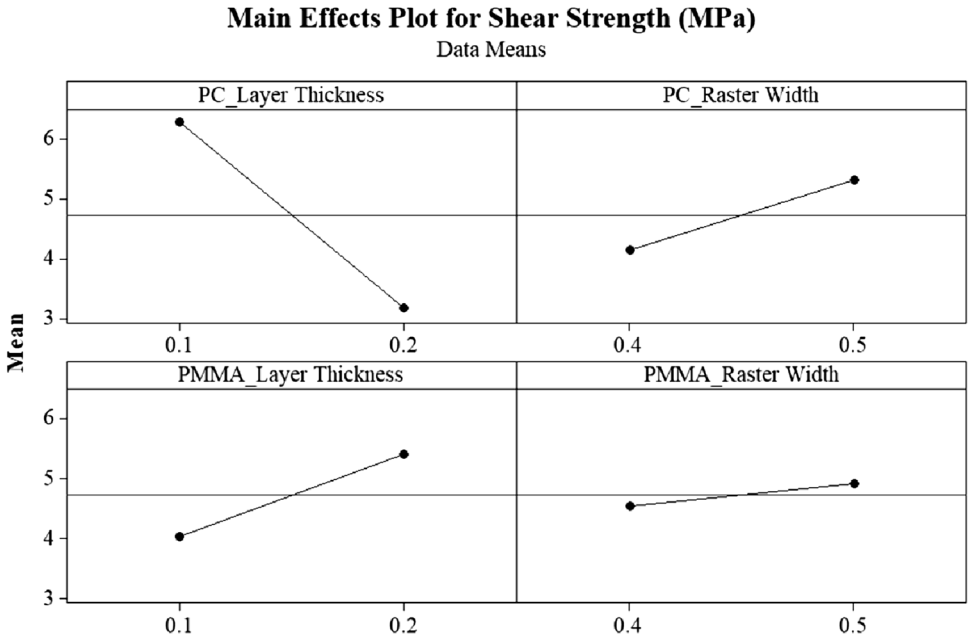

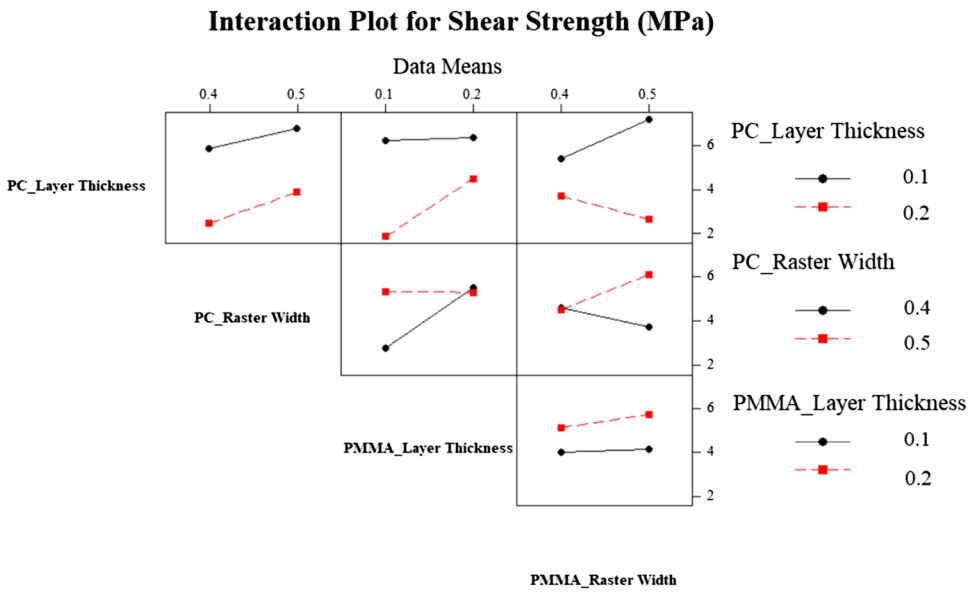

Fig. 13 Interaction plot of the factors of the PC/PMMA specimens

interface failure, similar to the aforementioned runs, whilst others exhibited layer-tear failure. Run 7 consisted of specimens A and C experiencing layer-tear failure with some PC residue at the PMMA corner, whilst specimen B had most of the PMMA sheared off along with the PC as shown in Fig. 14. Despite variations in shear strength values, run 7 specimen B had the highest average shear strength amongst all runs. The lower force and strength in specimens A and C could be attributed to interface defects caused by PC residue. Greater overall thicknesses correlated with better interface bonding and increased shear strength.

3.4.2 Lap-shear tests of PMMA/PC

All the specimens of the PMMA/PC printing order experienced stock-break failure, i.e. the PMMA/PC interfacial bonding strength was greater than the tensile strength of PMMA as shown in Fig. 15. This is because the PC's higher extrusion temperature of 250 °C and PMMA's lower glass transition temperature T_g of 90 °C, aided in polymer chain diffusion and entanglement. The PC's molecular chains remained mobile and could easily diffuse into the PMMA during printing because of its greater extrusion temperature, whereas PMMA's lower T_g enabled the PMMA macromolecules to become mobile whilst the first PC layer was being printed.

Although all the specimens failed in stock-break failure mode, different ultimate tensile strength values were achieved due to the process parameters which fabricated the PMMA in the different runs. Greater ultimate tensile strength values were achieved when the specimens were fabricated with a layer thickness of 0.1 mm such as ones from runs 2, 7, and 8. Compression of the layers occurred since more layers were deposited which reduced voids or air gaps between the layers. These runs also attained the greatest average thicknesses, which may have contributed to obtaining high tensile strength due to the additional mechanical adhesion and interlocking at the interface. The lowest and highest tensile strength obtained were 5.445 MPa and 27.9 Mpa, respectively, which means 8.4% and 42.9% of the

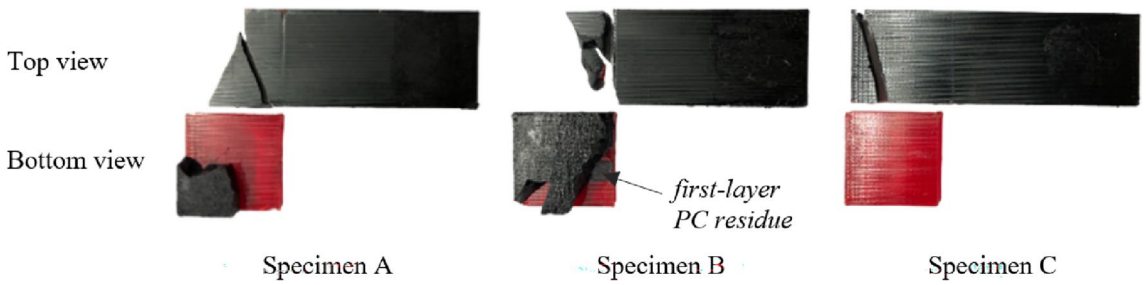

Fig. 14 Failure pattern of Run 7 specimens made of PC (black) and PMMA (red) illustrating the layer-tear failure of specimen A and C, and the first-layer PC residue on PMMA of specimen B

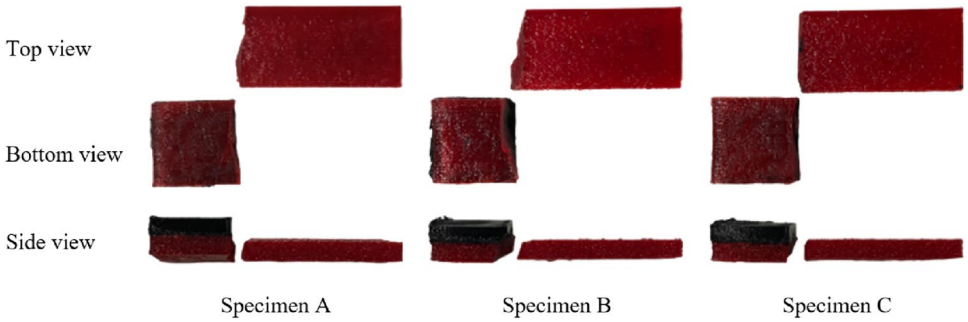

Fig. 15 Failure pattern of Run 7 specimens made of PMMA (red) and PC (black) illustrating the PMMA stock-break failure of all specimens

tensile strength of PMMA, which according to its material datasheet is 65 MPa [21].

3.5 Influence of contact area

Since the PMMA/PC specimens obtained the highest interface bonding, the process parameters of run 6 were selected as the most optimal run, in terms of dimensional and thickness accuracy. Therefore, three specimens with a reduced overlapping area of 15×15 mm^2 were fabricated. However, stock-break failure occurred at the cross-section of the PMMA (Fig. 16a); hence, there was no effect on the contact area as shear strength was still greater than the tensile strength of PMMA.

The area was further reduced to 5×5 mm^2 where layer-tear failure mode occurred in the three specimens with some of the PMMA sheared off with the peeled off PC material as can be seen in Fig. 16b. The specimens experienced such a failure mode since the force required for layer-tear failure is lower than for stock-break failure of PMMA, due to the smaller contact area, provided that the same interface bonding was achieved. It could be assumed that a similar material diffusion occurred as in the DOE PMMA/PC specimens, which resulted in a high interface bonding.

3.6 Printing approach

The printing simulation of the Design A specimen showed that the order of printing the layers consisted of printing the area where shearing was going to occur using the second material, followed by printing the tab, i.e. the clamping area. This decreased the time required to print the interface to be tested. Interface bonding is affected by which layer is printed first, as the temperature of the previous layer using the first material would be higher, enabling a better bond between the two materials. This design required the use of either support material or the addition of a bridge. However, a bridge was selected to reduce the post-processing and removal of the support material. High interface bonding was obtained with this design but was not practical due to overhanging of the material printed second. Stock-break failure of the PC occurred, namely at the overhanging area (Fig. 17), where only 2.15% and 2.68% of PC's tensile strength was obtained. This low strength could be related to the hygroscopic property of PC, which may have absorbed moisture during printing despite filaments pre-drying but due to the relatively long printing time and lack of printing enclosure. In addition, the extruder nozzle was required to move along the entire specimen and not only the overlapping shear area.

4 Conclusions

The aim of this work was achieved through the development of new test specimens for the characterisation of MMAM parts by FFF to determine the influencing factors on the interface strength. The test results showed that the PC/PMMA specimens were more dimensionally accurate than the PMMA/PC specimens. Three failure pattern modes were accomplished throughout all the specimens based on the DOE, including interface failure, layer-tear failure, or stock-break failure. Lap-shear testing showed

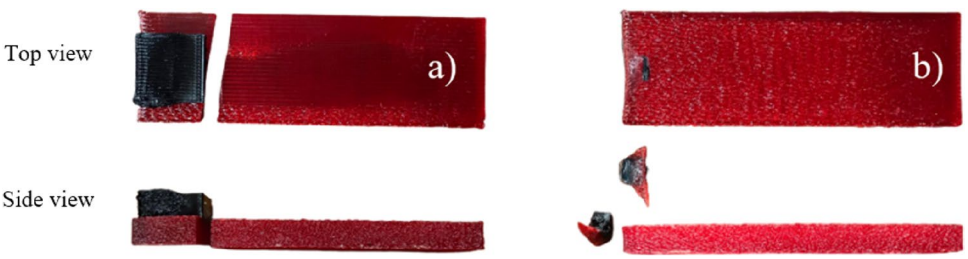

Fig. 16 Failure pattern of Run 6 specimen made of PMMA (red) and PC (black) with a reduced overlapping area to **a** 15×15 mm^2 still resulting in a stock-break failure of the PMMA, and to **b** 5×5 mm^2 leading to a layer-tear failure caused by a too small overlapping area

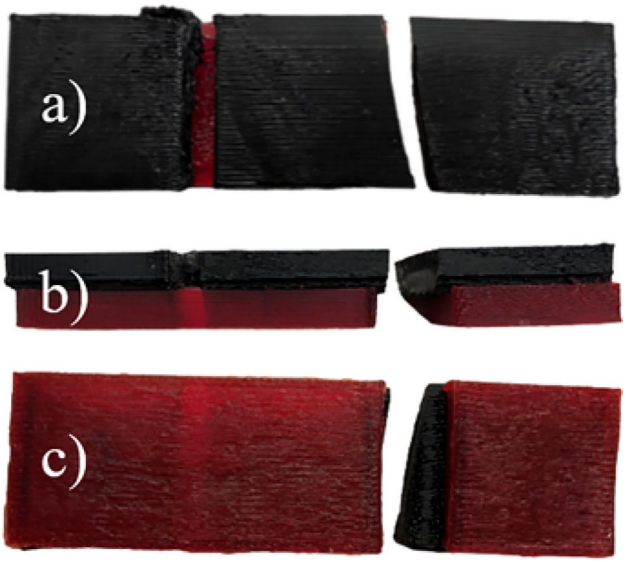

Fig. 17 Failure pattern of all the Design A test specimens showing **a** top, **b** side, and **c** bottom views where fracture occurred at the overhanging area

that the PC/PMMA specimens with lower layer thicknesses and higher raster widths resulted in higher interface bonding and shear strength. Regarding the PMMA/PC specimens, the interface bonding was greater than the tensile strength of the PMMA material, resulting in a stock-break failure mode.

Overall, the printing order of the material pair selected did influence the properties and interface strength of the specimens. However, the overlapping area did not have an influence on the PMMA/PC specimens as high shear strength was obtained, although the thickness and surface roughness of the specimens may have provided additional bonding for mechanical adhesion. Finally, careful consideration must be given to the specimen design in FFF MMAM.

For future work, additional work and improvements using the same material pair may be carried out. These include analysing further the causes of the low tensile strength, determining different ways to shear the PMMA/PC specimens, determining quantitative values, and the effects of the surface roughness on the interface bonding, analysing the fracture modes at the interfaces, creating a full factorial DOE, and applying the results to print real parts.

Funding Open Access funding provided by the University of Malta.

Data availability Data will be made available on request.

Declarations

Conflict of interest The authors declare that there is no conflict of interest.

References

1. 'ISO/ASTM 52900:2015', ISO. Accessed 18 Jul 2023. https://www.iso.org/standard/69669.html
2. Brancewicz-Steinmetz E, Sawicki J, Byczkowska P (2021) The influence of 3D printing parameters on adhesion between polylactic acid (PLA) and thermoplastic polyurethane (TPU). Materials. https://doi.org/10.3390/ma14216464
3. García-Collado A, Blanco JM, Gupta M, Dorado R (2021) Advances in polymers based multi-material additive-manufacturing techniques: state-of-art review on properties and applications. Addit Manuf 50:1–15. https://doi.org/10.1016/j.addma.2021.102577
4. Hasanov S et al (2022) Review on additive manufacturing of multi-material parts: progress and challenges. J Manuf Mater Process. https://doi.org/10.3390/jmmp6010004
5. Li H, Wang T, Sun J, Yu Z (2018) The effect of process parameters in fused deposition modelling on bonding degree and mechanical properties. Rapid Prototyp J 24(1):80–92. https://doi.org/10.1108/RPJ-06-2016-0090
6. Rajpurohit SR, Dave HK (2019) Analysis of tensile strength of a fused filament fabricated PLA part using an open-source 3D printer. Int J Adv Manuf Technol 101(5):1525–1536. https://doi.org/10.1007/s00170-018-3047-x
7. Tamburrino F, Graziosi S, Bordegoni M (2019) The influence of slicing parameters on the multi-material adhesion mechanisms of FDM printed parts: an exploratory study. Virtual Phys Prototyp 14(4):316–332. https://doi.org/10.1080/17452759.2019.1607758
8. Watschke H, Waalkes L, Schumacher C, Vietor T (2018) Development of novel test specimens for characterization of multi-material parts manufactured by material extrusion. Appl Sci 8(8):1220. https://doi.org/10.3390/app8081220
9. Yap P-V, Chan M-Y, Koay S-C (2021) Preliminary study on mechanical properties of 3D printed multimaterials ABS/PC parts: effect of printing parameters. J Phys Sci 32(2):87–104. https://doi.org/10.21315/jps2021.32.2.7
10. Freund R, Watschke H, Heubach J, Vietor T (2019) Determination of influencing factors on interface strength of additively manufactured multi-material parts by material extrusion. Appl Sci. https://doi.org/10.3390/app9091782
11. O'Donnell F, Duffy A, Cad Centre (1998) A design research approach. pp 1–9
12. Fang L, Yan Y, Agarwal O, Yao S, Seppala J, Kang S (2020) Effects of environmental temperature and humidity on the geometry and strength of polycarbonate specimens prepared

by fused filament fabrication. Mater Basel Switz. https://doi.org/10.3390/ma13194414
13. Goff J, Whelan T (1988) The Dynisco extrusion processors handbook, 2nd edn. Dynisco Incorporated, Franklin
14. Guedes Pinto AM, Magalhães AG, Gomes da Silva F, Monteiro Baptista AP (2008) Shear strength of adhesively bonded polyolefins with minimal surface preparation. Int J Adhes Adhes 28(8):452–456. https://doi.org/10.1016/j.ijadhadh.2008.04.003
15. HK Dave, JP Davim (2021) Fused deposition modeling based 3D printing. Springer, Berlin
16. 'ToolChanger & Motion System Bundle inc Tools & Hemera Extruders', E3D Online. https://e3d-online.com/products/toolchanger-hemera-bundle. Accessed 5 Nov 2022
17. Dwamena M 'How to get the perfect line width settings in 3D printing', 3D Printerly. https://3dprinterly.com/how-to-get-the-perfect-layer-height-setting/. Accessed 3 Dec 2022
18. ISO 527-1:2012, Switzerland. https://www.iso.org/standard/56045.html. Accessed 11 Apr 2023
19. Quini J, Marinucci G (2012) Polyurethane structural adhesives applied in automotive composite joints. Mater Res 15:434–439. https://doi.org/10.1590/S1516-14392012005000042
20. ePC(Polycarbonate) (2021) https://www.esun3d.com/epc-product/. Accessed 27 Jan 2023
21. Devil Design Download Product card-PMMA. https://devildesign.com/en/do-pobrania/. Accessed 27 Jan 2023